Dependence of the Absorption and Optical Surface Plasmon Scattering of MoS_2 Nanoparticles on Aspect Ratio, Size, and Media

Lena Yadgarov,[†] Charina L. Choi,[‡] Anastasiya Sedova,[†] Ayala Cohen,[§] Rita Rosentsveig,[†] Omri Bar-Elli,[⊥] Dan Oron,[⊥] Hongjie Dai,[‡] and Reshef Tenne[†,*]

[†]Department of Materials and Interfaces, Weizmann Institute of Science, Rehovot 76100, Israel, [‡]Department of Chemistry, Stanford University, Stanford, California 94305-5080, United States, [§]Department of Materials Engineering, Ben Gurion University, Beer Sheva, Israel, and [⊥]Department of Physics of Complex Systems, Weizmann Institute of Science, Rehovot 76100, Israel

ABSTRACT The optical and electronic properties of suspensions of inorganic fullerene-like nanoparticles of MoS_2 are studied through light absorption and zeta-potential measurements and compared to those of the corresponding microscopic platelets. The total extinction measurements show that, in addition to excitonic peaks and the indirect band gap transition, a new peak is observed at 700–800 nm. This spectral peak has not been reported previously for MoS_2. Comparison of the total extinction and decoupled absorption spectrum indicates that this peak largely originates from scattering. Furthermore, the dependence of this peak on nanoparticle size, shape, and surface charge, as well as solvent refractive index, suggests that this transition arises from a plasmon resonance.

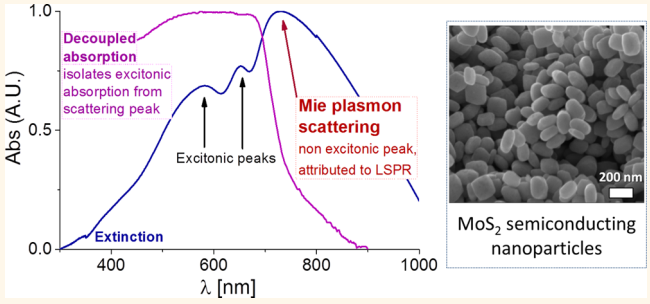

KEYWORDS: surface plasmon scattering · aspect ratio · MoS_2 · inorganic fullerene-like nanostructures · semiconducting nanoparticles

The first inorganic compounds to exhibit fullerene-like (denoted IF) structures and nanotubes (INT) were the layered metal dichalcogenides MX_2 (M Mo/W; X S/Se).[1,2] The large-scale synthesis of IF-MS_2 nanoparticles (NPs)[3,4] and WS_2 nanotubes[5] led to a considerable amount of research related to the structural, mechanical, optical, and electronic properties of these nanomaterials. These studies have demonstrated numerous applications, most notably their use as solid lubricants.

A recent surge of interest in layered metal dichalcogenides has provided evidence for high field-effect mobility[6] and luminescence[7] in easily exfoliated[8] single-layer MoS_2. These remarkable results caused a renewed interest in inorganic layered nanomaterials, including INT and IF. For example, unzipping WS_2 nanotubes results in few-layer WS_2 flakes with many active edge sites for hydrogen evolution catalysis.[9]

The IF nanostructures consist of 30–40 concentric MS_2 shells and have an average size of 70 to 200 nm (depending on the synthetic conditions). Transmission and scanning electron microscopy (TEM and SEM) analyses reveal that the IF-MoS_2 NPs deviate from a perfect spherical shape and in fact are somewhat oblate (see Figure 1).

Both MoS_2 and WS_2 are semiconductors with an indirect band gap of approximately 1.2[10] and 1.3 eV,[11] respectively. The IF/INT-MS_2 NPs were shown to preserve their bulk semiconducting behavior.[12,13] However, as a result of intrinsic defects in the MoS_2 layers, new energy states appearing within the band gap of the semiconducting MoS_2 may arise.[14] These minor defects and dislocations in the NP lattice can induce excess charge carriers which are trapped at the MS_2 nanoparticle surface, particularly in suspensions where different redox species may lead to extra charges residing at these surface sites. The charge carriers on the surface

* Address correspondence to reshef.tenne@weizmann.ac.il.

Received for review January 3, 2014 and accepted March 26, 2014.

Published online March 26, 2014
10.1021/nn5000354

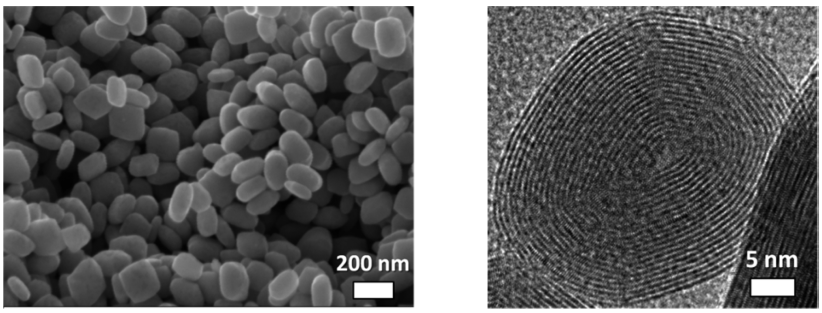

Figure 1. SEM (left) and TEM (right) images of IF-MoS_2 NPs.

should induce charged colloidal behavior of the MS_2 nanoparticles in solutions.

The effect of excess charge carriers on the NP surface can be analyzed using zeta-potential (ZP) measurements.[15] However, it is important to note that ZP measurements are suitable mostly for round particles. Thus, in the present work, the ZP measurements are limited to the IF nanoparticles and they are not compared to a bulk counterpart (*i.e.*, microscopic 2H-MoS_2 platelets). Here, 2H stands for a unit cell with hexagonal symmetry consisting of a repeat unit made of two MoS_2 layers with honeycomb structure.

The shape and size of NPs have a distinct effect on the resulting optical and electronic properties.[16−21] Colloidal solutions of noble metal NPs like silver and gold exhibit a very intense color, which is not present in the bulk material or the individual atoms. This intense color is attributed to absorption and scattering by surface plasmons, in which collective oscillations of the free carriers are induced by interactions with an electromagnetic field.[20]

The theory developed by Mie[22] considered the surface plasmon resonance for spherical particles of different sizes. Later, it was shown that the surface plasmon absorption of gold NPs exhibits a red shift with increasing NP size, while the bandwidth increases in the size range above 20 nm.[23−25] For large NPs, the extinction cross section is reliant on higher-order multiple modes in the Mie equation.[22] Thus, the extinction spectrum is dominated by quadrupole and octupole absorption as well as by scattering.[23,26,27] Since the higher oscillation modes depend on the particle shape and size, the plasmon absorption maximum is red-shifted and the bandwidth increases with the NP size. The total extinction is then the superposition of all contributing multiple oscillations peaking at different energies. Recently, there has been a growing interest in localized surface plasmon resonance (LSPR) spectroscopy of doped semiconductor nanocrystals. This is a relatively newly discovered phenomenon and serves as a clear optical signature of mobile charge carriers.[28] Unlike many other methods, studying LSPR phenomena allows the design of easy and accessible setup for measurements of redox chemistry[29,30] and photoelectrochemistry,[31] sensing of crystallographic phases,[32] and more.

Quantum size effects of the IF-MoS_2 NPs are minor due to their large size (diameter is 70−200 nm). However, the optical properties of these NPs are affected by strain (distortion of the bonds), with a distinct red shift of the excitonic spectra for NPs relative to the bulk material.[13,33,34] In addition to the excitonic peaks, we show here that an additional transition at ~700−800 nm is observed in the total extinction spectra of IF-MoS_2 suspensions. Some of the methods used to assign the observed peak to LSPR are size dependence, sensitivity to the medium refractive index, interparticle coupling, and shape anisotropy effects (aspect ratio).[28] Indeed, the observed non-excitonic peak exhibits a significant red shift and broadening with increasing NP size, surface charge, and solvent refractive index and can be attributed to Mie plasmon scattering. This is further supported by ZP measurements, which confirmed that the IF NPs have a distinct negative surface charge. In contrast to the IF NPs, the (2H) MoS_2 platelets do not show a distinguishable scattering peak, but rather a plateau.

RESULTS AND DISCUSSION

Figure 2a provides a direct comparison between the UV−vis extinction measurement and the decoupled light absorption spectrum of both IFs and platelets. Clearly, the extinction peak at 730 nm (Figure 2a, curve β) is primarily due to scattering rather than absorption. In fact, a large scattering cross section relative to the absorption cross section is expected for large NPs of this size.[29] The apparent scattering peak at 730 nm is considerably red-shifted when compared to the A exciton absorption (650 nm).[13] The intensity of the A exciton should be lower or equal to that of the B exciton;[35] thus, the high intensity of the lowest wavelength peak also indicates that it cannot be assigned to an excitonic peak. The large intensity of this scattering peak leads to a significant distortion in the intensity and location of the exciton's peaks. These observations support the attribution of this peak (730 nm) to a surface plasmon resonance scattering process, described by Mie in 1908.[22]

Originally, Mie developed his scattering theory[22] for metallic NPs with carrier density up to 10^{22} cm^{-3}. However, according to Luther *et al.*,[36] a surface

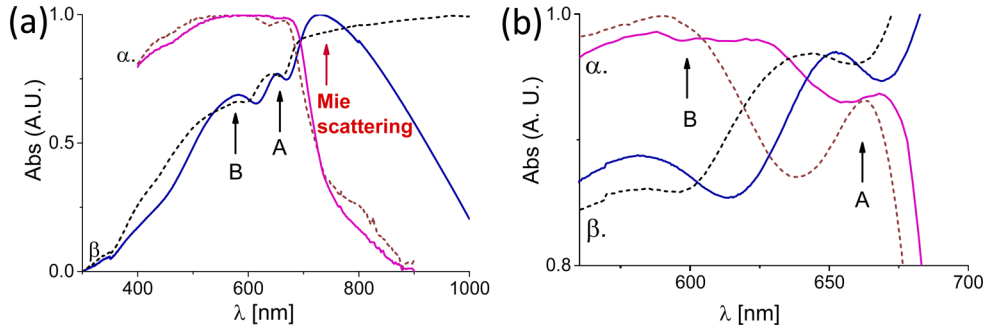

Figure 2. (a) UV−vis and integrating sphere (Quantaurus-QY) spectra of IF-MoS_2 (solid line) and 2H-MoS_2 suspensions (dashed line). The curve marked as α is the decoupled absorption measured by the integrating sphere Quantaurus QY; β is the extinction measured by Cary-5000 UV−vis spectrometer. Excitons A and B of the IF are red-shifted compared to the platelets. (b) Magnification of the excitonic peaks. ***Note that absorption spectrum (α) of the platelets (dashed line) in panel a shows some absorption at ∼800 nm. This peak is an artifact which accrues due to the poor distribution of the platelets in aqueous solutions.***

plasmon scattering peak in semiconducting NPs will appear in the infrared region given electron or hole carrier densities in the range of 10^{19}−10^{22} cm^{-3}. The LSPR frequency dependence on free carrier density can be estimated using equation 1[23] (note that the Drude model and oblate shaped NPs are assumed here).

$$\omega_{sp}^2 = \frac{L}{\varepsilon_m - L(\varepsilon_m - 1)} \frac{n \cdot e^2}{\varepsilon_0 \cdot m_e^*} \quad (1)$$

$$L_1 = \frac{g(r)}{2r^2}\left[\frac{\pi}{2} - \arctan g(r)\right] - \frac{g^2(r)}{2}; \quad (1.2.1)$$

$$g(r) = \sqrt{\frac{1 - r^2}{r^2}}, \quad r^2 = 1 - \frac{c^2}{a^2}$$

$$L_2 = L_3 = \frac{1 - L_1}{2} \quad (1.2.2)$$

Here the frequency (ω_{sp}) is 2.58 × 10^{15} Hz (730 nm, Figure 2); the medium dielectric constant ε_m is set as 1.77 for water, and the effective mass of the free carrier m_e^* is 0.45m_e[37] (m_e is the effective mass of a free electron); e is the electron charge, and ε_0 is the permittivity of free space. Assuming oblate shaped NPs, the shape factors ($L_{1,2}$) are derived as specified in equation 1.2.1 where a and c are the particle dimensions.[38] Using the measured LSPR frequency, the free carrier concentration (n) is estimated as ∼10^{21} cm^{-3}. This estimation of the carrier concentration is rather high, but one should bear in mind the fact that the Drude model often overestimates the carrier density for nanomaterials and is not suited for accurate calculations.[28]

The free carrier density of unintentionally doped INT-WS_2[39] is 10^{19} cm^{-3}. This large free carrier density is possibly the result of the high-temperature synthesis (*ca.* 840 °C) and reflects the higher volatility of the sulfur atoms (sulfur vacancies). The reaction conditions for the IF-MoS_2 are similar to the above, and hence its free carrier density is not expected to be lower. Recently, it was shown that the intrinsic defects in the MoS_2 layers may induce new energy states within its band gap.[14] These dislocations and defects in the lattice can induce excess charge carriers which are trapped on the NP surface, especially when suspended in solutions and in contact with redox species, such as dissolved gases: OH^- moieties, organic moieties, such as HCO_2^-, *etc*. Furthermore, the IF NPs likely have many more strain-related defects[40] than the INT-WS_2. When all of the above are considered, the carrier density of the IF is expected to be higher than that of the INT. Another reason for high free carrier density of the IF NPs could be the charge buildup which is induced by the UV−vis light irradiation.[28,41−43] It is noteworthy that very high carrier concentrations have already been observed in other colloidal systems. For instance, like for the IF NPs, in ZnO semiconducting NPs, this charge buildup resulted in an LSPR absorption band in the NIR region.[44] The excess electron concentration deduced from the LSPR frequency is ∼$10^{20}$$cm^{-3}$, well above the suggested Mott density (6 × $10^{18}$$cm^{-3}$) of ZnO.[44] Thus, the calculated free carrier concentration of IF NPs (10^{21} cm^{-3}) is further confirmation that the observed scattering peak is consistent with the assignment of a surface plasmon.

The spectra presented in Figure 2 and the LSPR calculation indicate that the Mie scattering mechanism is also relevant to the IF-MoS_2 NPs. The spectrum of the highly anisotropic 2H platelets does not show a distinguishable scattering peak, but rather a (scattering) plateau beyond 683 nm. The broad scattering of the platelet suspension may arise from various factors including highly anisotropic structure, poor dispersion of the particles in aqueous solution, extremely damaged and oxidized surfaces, and rapid agglomeration of the 2H-MoS_2 platelets, all contributing to the large inhomogeneity in the scattering process. The average size of the platelets inspected here is about 2 μm. However, it is not improbable that a more significant scattering effect may take place in measurement of smaller (200−500 nm) platelets and in particular in suspensions of exfoliated MoS_2 nanoslabs.

The decoupled absorption spectrum (Figure a, curve α) allows isolation of the excitonic absorption

from the scattering peak. A closer view of these spectra (Figure 2b) reveals that excitonic absorption transitions appear red-shifted from the UV−vis extinction spectra. The main reason for that shift is the convolution of scattering and absorption processes in the UV−vis extinction measurements. It is important to note that, although the decoupled absorption measurement provides the exciton's position quite precisely, there is nevertheless a few nanometer measurement error, due to the low contrast of the A exciton absorption peak, as discussed below.[45]

In the early extinction measurements of IF-MoS_2 thin films,[13] scattering effects were largely diminished. However, a tailing of the extinction edge to lower energies was observed and attributed to the large size and shape distribution of the NPs. At present, with the availability of more uniform IF samples,[4,5] a more precise determination of the excitonic peaks and decoupling of the absorption and scattering effects is possible in solutions of these NPs. The A and B excitons of IF NPs are red-shifted with respect to the 2H platelets (Table 1). The red shift can be ascribed to the intralayer structural strains.[13,33,34,46−50] The 12 meV red shift of exciton A compared to the 33 meV shift of the B exciton indicates that the latter is more sensitive to confinement and is strongly perturbed by formation of the IF structure.[33]

It is important to note that, due to the large intensity of the scattering peak, the estimation of the excitons' location using the UV−vis spectra of the NP suspensions is highly inaccurate (Figure 1, curve β). Interestingly, when the absorbance spectrum is obtained without the scattering distortion (Figure 1, curve α), resolving the excitonic peaks becomes even more challenging. The phenomenon of the excitonic peak distortion and quenching is a result of the high free carrier concentration of the NPs.[28,51] For example, for ZnO NPs discussed above, the excess electron concentration is $\sim 10^{20}$ cm^{-3}. Thus bound electron−hole excitonic states cannot be sustained due to the high dielectric screening.[28,44] This occurrence clarifies the excitonic band bleaching in the charged state of ZnO NPs, a well-known occurrence.[41,43] A similar phenomenon was recently observed for MoS_2 monolayer, where, due to the high doping density ($\sim 10^{13}$ cm^{-2}), significant suppression of the excitonic peaks occurs.[51] Note that this free carrier concentration for a single MoS_2 layer in these case corresponds to a bulk density of about $\sim 1.5 \times 10^{20}$ cm^{-3} (10^{13} $cm^{-2}/6.5 \times 10^{-8}$ cm)[6] It was revealed that, as the electron doping increases, the absorbance of the A exciton nearly disappears and the A^- feature is broadened.[51] This was accompanied by a small blue shift of the A exciton absorption peak.

The spin−orbit splitting (Δ) was estimated from the difference in the peak positions of the A and B excitons (Table 1) and was found to be Δ = 0.235 and 0.214 eV for 2H- and IF-MoS_2, respectively. This difference indicates that the band curvature at the K-point is modified by the structural strain[33] in the IF NPs when compared to platelets. The value of the spin−orbit splitting is lower than that observed in prior reports[33,47] by ~50 meV, which is attributed to structural variations in different batches of measured MoS_2 and dissimilar measurements' setups.

The direct gap ($E_{g,dir}$) of MoS_2 is split by the A and B excitons[47,48] and can be estimated by equation 2.[50]

$$E_{g,dir} = E_A + E_{Ryd} \quad (2)$$

where E_A is the A exciton energy and E_{Ryd} = 0.042 eV is the exciton Rydberg constant.[52] The results of these calculations are presented in Table 1 and are in good agreement with previous experiments.[50,53] The decrease of the direct band gap ($E_{g,dir}$) of the IF compared to the 2H platelets is attributed to strain and confinement effects.[48]

The indirect band gap was calculated as described by Pankove[54] using the absorption measurements (Figure 2, curve α) and the following equation 3.

$$\alpha = \frac{A(h\nu - E_g)^2}{h\nu} \quad (3)$$

Here α is the absorption coefficient, A is a constant, and E_g is the indirect band gap of the semiconductor. As presented in Table 1, the calculated indirect band gap of the IF NPs (1.24 eV) is higher than that of 2H platelets (1.03 eV) but is similar to the one reported for a single crystal (1.23 eV[55]). The low E_g value of the platelets can be attributed to the inhomogeneity of the measured suspension. This inhomogeneity appears due to the rapid agglomeration of the platelets in the solution and may cause low and anisotropic absorption. Also, the exciting light is incident on the platelets exposing both

TABLE 1. Summary of Band Gaps and Exciton Peak Positions Measured for Various Compounds in This Study[a]

		exciton [eV]			band gap [eV]	
	scattering peak [eV]	A	B	spin−orbit splitting [eV]	indirect	direct
platelets 2H-MoS_2	plateau	1.879[b]	2.114[b]	0.235[b]	1.033[b]	1.921[b]
		(1.880[53])	*(2.060[53])*	*(0.180[53])*	*(1.06[62])*	
IF-MoS_2	1.698[c]	1.867[b]	2.081[b]	0.214[b]	1.243[b]	1.909[b]
		(1.846[50])	*(2.005[50])*	*(0.159[50])*		*(1.888[50])*

[a] Literature values are given in parentheses. Note that all the results from ref 53 are measured at 77 K. [b] Absorption measured by Quantaurus-QY (integrating sphere). [c] Absorption measured by UV−vis spectrophotometer.

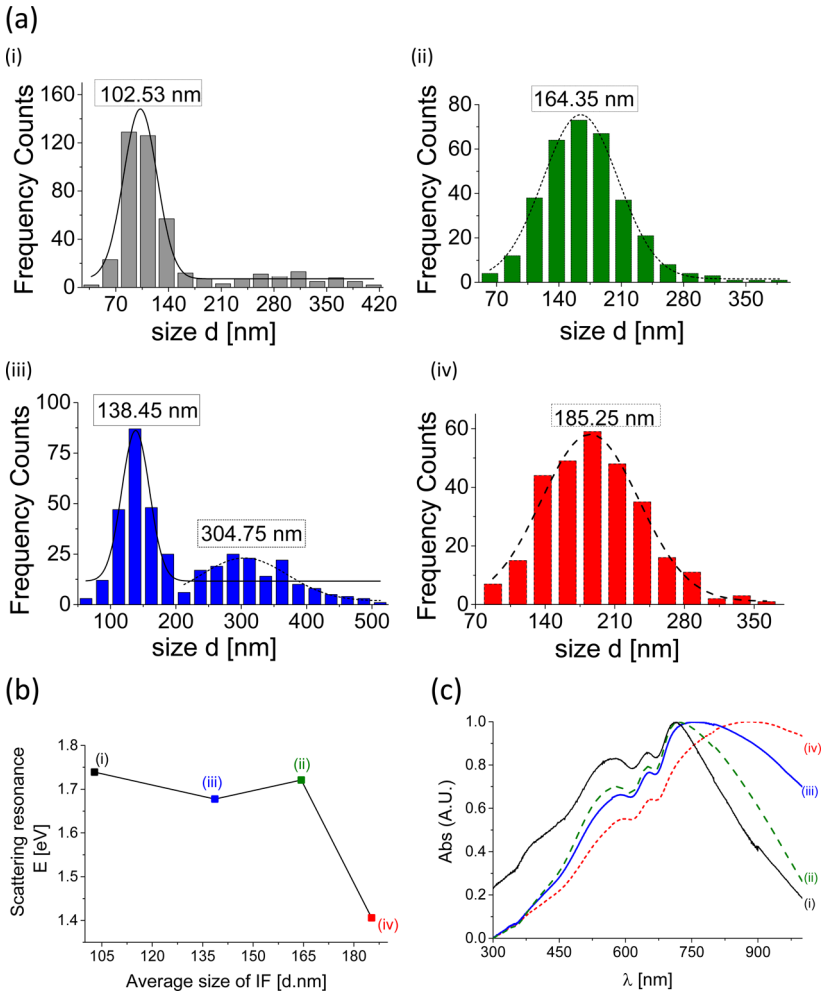

Figure 3. (a) Size distribution (diameter) of the IF NPs. The dashed line is the Gauss fit. (b) Influence of the NP size on the surface plasmon peak energy. (c) UV−vis spectra of different IF-MoS_2 batches with various sizes. Notation i to iv in (a−c) refers to the NP batch. ***Note that the NPs examined as the function of RI are similar to batch i, and the NPs examined as the function of pH and for ZP measurements are similar to NP batch ii.***

the basal (001) and the prismatic (*hk*0) surfaces, each having different optical properties. Consequently, the absorption cross section is sensitive to the sizes and shape of the particles and affects the value of the determined gap. In the case of the IF NPs, as well as for crystal, the light is incident only on the basal (001) surface.

Figures 3−5 summarize how the scattering peak of the IF-MoS_2 suspensions is influenced by the solution refractive index, pH, and the particle size. The extinction presented in Figure 3c, 4b, and 5b is the superposition of all contributing multiple oscillations peaking at different energies.[23−27]

As the size, size distribution, and aspect ratio of the NPs increase, the scattering peak is broadened and is red-shifted (Figure 3b,c). These effects can be ascribed to the increased contribution of higher oscillation modes, like quadrupoles, for larger and more asymmetric nanoparticles.[22] The size distribution of the various samples used is presented in Figure 3a, and the aspect ratio is presented in Table 2. Note that aspect ratio is defined here as the relative ratio of the major optical axis to the minor one (A/B) and is 1.00 for the spherical NPs. As expected, the NP with the lowest aspect ratio and size (batch i) has the narrowest scattering peaks with the highest energy. Likewise, the highest aspect ratio and size (batch iv) resulted in the broadest scattering peaks with the lowest energy. The NPs of batch ii are bigger than those of batch i; however, due to the comparable aspect ratios (2.94 for i and 2.83 for ii), their scattering peak energies are similar.[23,47] The scattering peak of NP batch iii is much broader when compared to that of batch ii due to its broad (bimodal) size distribution (Figure 3a,iii). The scattering peak of the NP of batch iv is considerably red-shifted and broadened when compared to that of batch i due to its larger size and aspect ratio. The exciton absorption peaks are also affected by the size of the NP and consequently by the number of MoS_2 layers. For example, the exciton peaks of the largest NPs are red-shifted when compared to the smallest NPs by ∼22 meV for A and ∼90 meV for B exciton peaks (Figure 3c). As the average IF size is larger, their distribution gets larger and the average number of

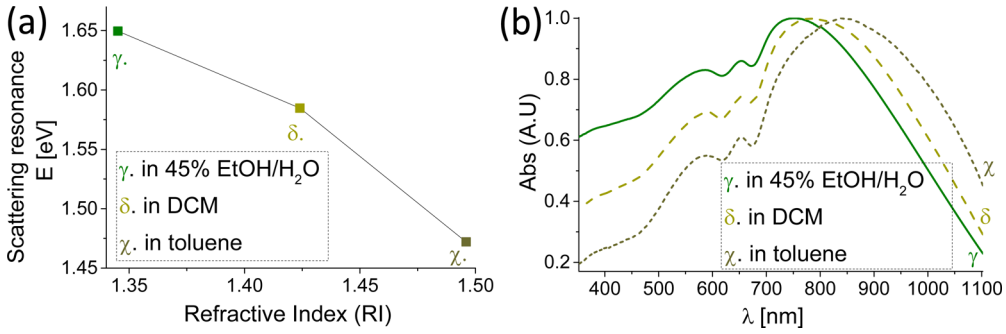

Figure 4. (a) Influence of the NP surrounding media (solvent refractive index) on the surface plasmon peak energy end (b) extinction spectra of the NP.

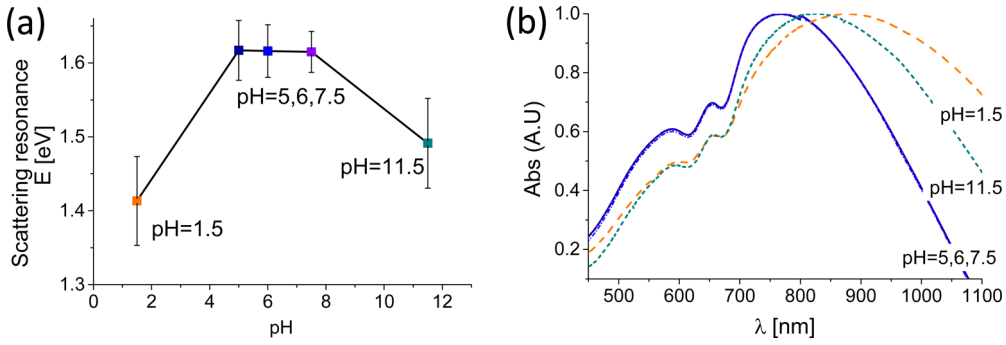

Figure 5. Influence of the surrounding pH on the (a) surface plasmon peak energy and (b) total extinction of the NP.

TABLE 2. Average Size, Thickness, and Aspect Ratio of the NP Batches i–iv[a]

	average diameter		average thickness		
batch number	nm	fwhm	nm	fwhm	aspect ratio
i	102.83	51.06	35.00	26.24	2.94
ii	164.35	99.50	58.12	43.97	2.83
iii (population 1)	138.45	49.72	42.20	29.68	3.28
iii (population 2)	304.75	156.28	85.00	3.53	3.59
iv	185.25	115.46	47.82	29.70	3.87

[a] Since the IF NPs have the shape of an oblate spheroid, the average diameter is the flattened side of the oblate and thickness is its narrowest side. Note that the average diameter of the NPs is derived from Gauss fit (Figure 3), thus full width at half-maximum (fwhm) can be addressed as the NP size distribution.

MoS_2 layers in the NPs increases. Hence, the effective exciton positions in the larger nanoparticles are softened, and the spin–orbit coupling is reduced.[33,50]

Information on how the surface plasmon resonance scattering depends on the surrounding medium can have practical ramifications since it provides a fundamental mechanism for signal detection in applications such as sensors and local imaging. Hence, it is important to understand the dependence of the plasmonic resonance on the refractive index (RI) of the surrounding media. To study the influence of the surrounding medium on the light scattering, the RI of the solvent was varied while keeping all other parameters including the nanoparticle batch the same.

Figure 4a,b summarizes the shift of the scattering peak energy with varying RI of surrounding medium. The red shift, typical of plasmonic scattering bands, is a clear consequence of eq 1, where the dielectric constant of the surrounding medium appears explicitly. Moreover, due to an inhomogeneous polarization of the NP by the electromagnetic field, the plasmon bandwidth increases as the wavelength of the interacting light becomes comparable to the NP dimension.[24] The broadening and red shift of the plasmon band is then generally attributed to retardation effects.[20] Notably, for the relatively large NPs in this study, and particularly considering their high refractive index, higher multipolar modes are expected to contribute more significantly as the RI of the surrounding medium is increased.[23,26] The RI dependence lends further evidence that the observed near-IR peak (730 nm) is due to plasmonic excitation.

The assessment of the pH influence on the surface scattering plasmon energy reveals that the narrowest width of the scattering peak is obtained when the pH of the suspension is in the range of 5–7.5 (Figure 5a,b). At this range, the position of the scattering peak remains unchanged (Figure 5a). At extreme pH values (1.5 and 11.5), the scattering peak is broadened and red-shifted. The results of ZP measurements (Figure 6) suggest that, when the pH is above 1.8, the NPs have negative surface charge. Thus it can be deduced that the peak broadening at pH = 1.5 is due to the overpassivation of extra charge on the NP surface by the protons. This passivation leads to agglomeration of the nanoparticles, as evidenced by their rapid precipitation. Indeed, the light scattering of the agglomerated

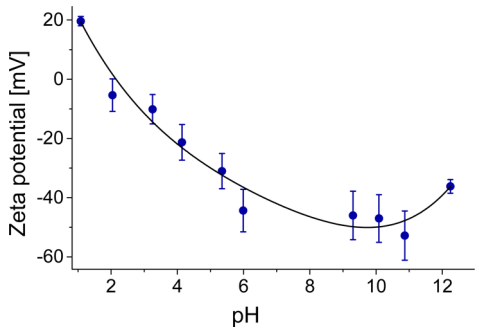

Figure 6. Zeta-potential *vs* pH for IF-MoS_2 nanoparticles.

nanoparticles is reminiscent of the platelet spectra in this range. When the pH is higher than 11, the Debye layer shrinks to a distance of a few nanometers,[56] which leads to a strong van der Waals attraction and precipitation of the agglomerated IF NPs. Alternatively, the large surface energy of the liquid leads to the floating of the IF NPs on its surface. Additional explanation for broadening and red shift of the scattering peak at extreme pH values (1.5 and 11.5) can be the interparticle coupling.[44] For instance, when spherical silver or gold NPs are brought into close proximity, the LSPR exhibits large red shifts due to the electromagnetic coupling of the plasmon resonances on nearby NPs.[57,58] It is important to note that, in view of all the above, it is clear that the pH does not influence the surface scattering peak as long as it is in the range of 5−7.5 (Figure 5a,b).

Measuring the surface potential of the NPs was somewhat challenging because the laser wavelength (632 nm) used for the ZP measurements coincides with the exciton A peak. Therefore, the laser light excites additional free carriers which are drifted or diffuse to the IF NP surface, modifying thereby the surface potential of the nanoparticle. This effect deserves a separate study which is underway. The calculated ZP values are based on a model which considers colloidal solutions of spherical nanoparticles. Since the 2H-MoS_2 platelets are not spherical and tend to sediment after 1−2 min, their surface potential could not be measured by the present method. In contrast, the IF NPs form quite a stable suspension in aqueous solution and do not precipitate for a few hours. The zeta-potential of the IF NPs measured as a function of pH is presented in Figure 6. The isoelectric point (IEP) according to these measurements appears at pH = 1.84, which is similar to the IEP of SiO_2.[59,60] The ZP of these nanoparticles is negative and remains almost unchanged between pH 5 and 11, which indicates the stability of this NP as a colloidal solution. When the pH is lower than 5, the ZP rapidly increases with decreasing pH. This behavior implies that in neutral solution the NPs acquire high negative surface charge which is probably associated with adsorbed moieties at the intrinsic defects of the curved MoS_2 layers of the NPs.

CONCLUSIONS

In conclusion, the UV−vis and integrating sphere measurements demonstrate a distinct Mie scattering peak in IF-MoS_2 suspensions. This scattering peak (730 nm) is believed to originate from a surface plasmon resonance scattering of the NP and is considerably red-shifted relative to the A exciton (650 nm). Using the measured LSPR frequency, the free carrier concentration is estimated as $\sim 10^{21}$ cm^{-3}. The origin of this high estimate can be the incompatibility of the Drude model for semiconducting nanomaterials.[28] Additional reasons for the high free carrier concentration might be sulfur vacancies in the NP, different defects in the MoS_2 layers[14] which are occupied by redox moieties from the supsension (or air), and charge buildup induced by the UV−vis light irradiation.[28] The spectrum of the anisotropically shaped 2H platelets shows a plateau in the IR range rather than a scattering peak. The positions of the A and B excitons of the IF are red-shifted in comparison to those in the 2H platelets. Nonetheless, since the bound electron−hole excitonic states cannot be sustained due to high free carrier concentration,[28,51] the excitonic peaks become highly distorted and quenched.

The scattering peak is red-shifted with increasing nanoparticle size, aspect ratio, and broadened with increase of their size distribution, consistent with the assignment to a surface plasmon mode. This peak also broadens and redshifts as the solvent refractive index increases, likely due to the enlargement of the NP effective size. At extreme pH, the scattering peak is shifted due to agglomeration and the inhomogeneous nature of the colloid suspension. However, as long as the pH is in the range of 5−7.5, it does not influence the scattering peak. The ZP measurements revealed that IF-MoS_2 have a high negative surface charge, which could be attributed to the dangling bonds or moieties adsorbed at the intrinsic defects of the curved MoS_2 layers. The low isoelectric point (pH = 1.84) and the highly negative ZP values indicate the stability of this NP as a colloidal solution.

MATERIALS AND METHODS

The IF-MoS_2 used in the current work were synthesized following the procedure reported by Rosentsveig *et al.*[4] The synthesis was carried out at 840 °C using MoO_3 as a precursor, and the resulting NPs were annealed for 20 h at 840 °C to remove the remaining oxide.[4] The XRD pattern of the annealed sample is presented in ref 4 and shows ~0.5% remaining oxide after the annealing process. These nanostructures' average size (70 to 200 nm) and number of MoS_2 shells depend on the synthetic conditions (see Table 2 and Figure 3a). TEM and SEM

analyses reveal that the IF-MoS_2 are somewhat oblate (Figure 1). Bulk 2H-MoS_2 powder was purchased from Aldrich and consisted of platelet shaped particles ($\sim 2\,\mu$m). The solutions for all the current measurements were prepared using purified water (Milli-Q RG, Millipore).

UV−vis extinction measurements were carried out on a Cary-5000 spectrometer (Varian). Samples were prepared by adding 0.6 mg of the MoS_2 platelets or IF NPs into 9 mL of purified water. The mixture was shaken by hand and then sonicated twice for 1−3 min using an ultrasonic bath. All suspensions were measured using quartz cuvettes. SEM and TEM analyses demonstrate that the IF NPs remain unaffected by this mild sonication procedure.

The position, width, and intensity of the scattering peak can be influenced by the solution refractive index, pH, and the particle size and its shape. To investigate the size dependence of scattering, three IF batches with varying particle sizes were examined. These IF batches were arbitrarily denoted as batch i, ii, and iii. In addition, the UV−vis spectra of the IF in different solvents were collected in order to understand the influence of the refractive index on the scattering effect. The solvents used for this series of measurements were ethanol in water 45% (v/v), dichloromethane (DCM), and toluene, with refractive indices of n = 1.33, 1.42, and 1.50, respectively. In order to elucidate the influence of pH on the optical extinction, the NPs were also measured in solutions with different pH values (1−12).

SEM was used to determine the average size of each examined batch of the IF NPs. Note that average size refers to the diameter of the oblate shaped IF NPs. The diameter here is the flattened side of the oblate NPs. Several images of each batch were taken, and ∼500 NPs from each batch were measured using ImageJ. Considering more than 500 NPs had no significant effect on the final results of this statistical analysis.

Decoupled absorption spectra, used to separate out scattering and absorption processes from the total extinction spectra, were measured using a Hamamatsu Quantaurus absolute QY system.[45,61] This instrument directly measures the amount of absorbed light by placing the sample inside an integrating sphere. The system was calibrated using a sample with known absorbance to extract the optical absorbance. A calibration for counting the single-pass absorption photons was performed to avoid the full extinction, which also includes photons that are scattered a few times before being detected.

The surface charge of the nanoparticles was determined through zeta-potential measurements using a ZetaSizer Nano ZS (Malvern Instruments Inc., UK) with a He−Ne light source (632 nm). To prepare the samples for these measurements, IFs (0.6 mg) were deagglomerated in 20 mL of purified water by sonicating for 5−10 min using an ultrasonic bath. Then 0.2 mL of the IF suspension was added to 1.5 mL of aqueous solutions with pH varying from 1 to 12 and sonicated for an extra 5 min. Before the addition of IF, the pH of each solution was adjusted using concentrated NaOH or HCl. The final concentration of the IF was 0.004 mg/mL. The solutions were measured in a folded capillary cell (DTS1060) made from polycarbonate with gold-plated beryllium/copper electrodes.

Conflict of Interest: The authors declare no competing financial interest.

Acknowledgment. This study was supported by an FTA grant from the Isr. Natl. Nanoinitiative; the Israel Science Foundation; ERC grant INTIF 226639, EU ITN 317451 grants and SINSLIM 258221. R.T. acknowledges the support of the Harold Perlman and the Irving and Azelle Waltcher Foundations in honor of Prof. M. Levy. He holds the Drake Family chair in Nanotechnology and is the director of the Helen and Martin Kimmel Center for Nanoscale Science. C.L.C. was supported by the National Science Foundation under Award No. CHE-1137395.

REFERENCES AND NOTES

1. Margulis, L.; Salitra, G.; Tenne, R.; Talianker, M. Nested Fullerene-like Structures. *Nature* **1993**, *365*, 113–114.
2. Tenne, R.; Margulis, L.; Genut, M.; Hodes, G. Polyhedral and Cylindrical Structures of WS_2. *Nature* **1992**, *360*, 444–445.
3. Feldman, Y.; Zak, A.; Popovitz-Biro, R.; Tenne, R. New Reactor for Production of Tungsten Disulfide Hollow Onion-like (Inorganic Fullerene-like) Nanoparticles. *Solid State Sci.* **2000**, *2*, 663–672.
4. Rosentsveig, R.; Margolin, A.; Gorodnev, A.; Popovitz-Biro, R.; Feldman, Y.; Rapoport, L.; Novema, Y.; Naveh, G.; Tenne, R. Synthesis of Fullerene-like MoS_2 Nanoparticles and Their Tribological Behavior. *J. Mater. Chem.* **2009**, *19*, 4368–4374.
5. Zak, A.; Sallacan-Ecker, L.; Margolin, A.; Genut, M.; Tenne, R. Insight into the Growth Mechanism of WS_2 Nanotubes in the Scaled-up Fluidized-Bed Reactor. *NANO* **2009**, *4*, 91–98.
6. Radisavljevic, B.; Radenovic, A.; Brivio, J.; Giacometti, V.; Kis, A. Single-Layer MoS_2 Transistors. *Nat. Nanotechnol.* **2011**, *6*, 147–150.
7. Mak, K. F.; Lee, C.; Hone, J.; Shan, J.; Heinz, T. F. Atomically Thin MoS_2: A New Direct-Gap Semiconductor. *Phys. Rev. Lett.* **2010**, *105*, 136805(4).
8. Coleman, J. N.; Lotya, M.; O'Neill, A.; Bergin, S. D.; King, P. J.; Khan, U.; Young, K.; Gaucher, A.; De, S.; Smith, R. J. Two-Dimensional Nanosheets Produced by Liquid Exfoliation of Layered Materials. *Science* **2011**, *331*, 568–571.
9. Choi, C. L.; Feng, J.; Li, Y.; Wu, J.; Zak, A.; Tenne, R.; Dai, H. WS_2 Nanoflakes from Nanotubes for Electrocatalysis. *Nano Res.* **2013**, *6*, 921–928.
10. Coehoorn, R.; Haas, C.; Dijkstra, J.; Flipse, C.; De Groot, R.; Wold, A. Electronic Structure of $MoSe_2$, MoS_2, and WSe_2. I. Band-Structure Calculations and Photoelectron Spectroscopy. *Phys. Rev. B* **1987**, *35*, 6195–6202.
11. Ballif, C.; Regula, M.; Schmid, P.; Remškar, M.; Sanjines, R.; Levy, F. Preparation and Characterization of Highly Oriented, Photoconducting WS_2 Thin Films. *Appl. Phys. A: Mater. Sci. Process.* **1996**, *62*, 543–546.
12. Yadgarov, L.; Rosentsveig, R.; Leitus, G.; Albu-Yaron, A.; Moshkovich, A.; Perfilyev, V.; Vasic, R.; Frenkel, A. I.; Enyashin, A. N.; Seifert, G.; Rapoport, L.; Tenne, R. Controlled Doping of MS_2 (M=W, Mo) Nanotubes and Fullerene-like Nanoparticles. *Angew. Chem., Int. Ed.* **2011**, *51*, 1148–1151.
13. Frey, G. L.; Tenne, R.; Matthews, M. J.; Dresselhaus, M. S.; Dresselhaus, G. Optical Properties of MS_2 (M= Mo, W) Inorganic Fullerene-like and Nanotube Material. *J. Mater. Res.* **1998**, *13*, 2412–2417.
14. Enyashin, A. N.; Bar-Sadan, M.; Houben, L.; Seifert, G. Line Defects in Molybdenum Disulfide Layers. *J. Phys. Chem. C* **2013**, *117*, 10842–10848.
15. Hunter, R. J. *Zeta Potential In Colloid Science: Principles and Applications*; Academic Press: London, 1981; Vol. 125.
16. Henglein, A. Physicochemical Properties of Small Metal Particles in Solution: "Microelectrode" Reactions, Chemisorption, Composite Metal Particles, and the Atom-to-Metal Transition. *J. Phys. Chem.* **1993**, *97*, 5457–5471.
17. Henglein, A. Small-Particle Research: Physicochemical Properties of Extremely Small Colloidal Metal and Semiconductor Particles. *Chem. Rev.* **1989**, *89*, 1861–1873.
18. Alivisatos, A. P.; Johnsson, K. P.; Peng, X.; Wilson, T. E.; Loweth, C. J.; Bruchez, M. P.; Schultz, P. G. Organization of 'Nanocrystal Molecules' Using DNA. *Nature* **1996**, *382*, 609–611.
19. Schmid, G. *Clusters And Colloids: From Theory to Applications*; John Wiley & Sons: New York, 1994.
20. Kreibig, U.; Vollmer, M. *Optical Properties of Metal Clusters*; Springer: Berlin, 1995; Vol. 25, p 535.
21. Perenboom, J.; Wyder, P.; Meier, F. Electronic Properties of Small Metallic Particles. *Phys. Rep.* **1981**, *78*, 173–292.
22. Mie, G. Pioneering Mathematical Description of Scattering by Spheres. *Ann. Phys* **1908**, *25*, 337.
23. Bohren, C. *Absorption and Scattering of Light by Small Particles*; Wiley: New York, 1983.
24. Link, S.; El-Sayed, M. A. Spectral Properties and Relaxation Dynamics of Surface Plasmon Electronic Oscillations in Gold and Silver Nanodots and Nanorods. *J. Phys. Chem. B* **1999**, *103*, 8410–8426.
25. Link, S.; El-Sayed, M. A. Shape and Size Dependence of Radiative, Non-radiative and Photothermal Properties of Gold Nanocrystals. *Int. Rev. Phys. Chem.* **2000**, *19*, 409–453.

26. Kerker, M. *The Scattering of Light, and Other Electromagnetic Radiation*; Academic Press: New York, 1969; Vol. 16, p 666.
27. Creighton, J.; Eadon, D. New Mixed Quantum/Semiclassical Propagation Method. *J. Chem. Soc., Faraday Trans.* **1991**, *87*, 3881–3891.
28. Faucheaux, J. A.; Stanton, A. L.; Jain, P. K. Plasmon Resonances of Semiconductor Nanocrystals: Physical Principles and New Opportunities. *J. Phys. Chem. Lett.* **2014**, *5*, 976–985.
29. Jain, P. K.; Manthiram, K.; Engel, J. H.; White, S. L.; Faucheaux, J. A.; Alivisatos, A. P. Doped Nanocrystals as Plasmonic Probes of Redox Chemistry. *Angew. Chem., Int. Ed.* **2013**, *52*, 13671–13675.
30. Guyot-Sionnest, P. Electrical Transport in Colloidal Quantum Dot Films. *J. Phys. Chem. Lett.* **2012**, *3*, 1169–1175.
31. Hirakawa, T.; Kamat, P. V. Charge Separation and Catalytic Activity of Ag@TiO_2 Core−Shell Composite Clusters under UV-Irradiation. *J. Am. Chem. Soc.* **2005**, *127*, 3928–3934.
32. Polking, M. J.; Jain, P. K.; Bekenstein, Y.; Banin, U.; Millo, O.; Ramesh, R.; Alivisatos, A. P. Controlling Localized Surface Plasmon Resonances in GeTe Nanoparticles Using an Amorphous-to-Crystalline Phase Transition. *Phys. Rev. Lett.* **2013**, *111*, 037401.
33. Frey, G. L.; Elani, S.; Homyonfer, M.; Feldman, Y.; Tenne, R. Optical-Absorption Spectra of Inorganic Fullerenelike MS_2 (M=Mo, W). *Phys. Rev. B* **1998**, *57*, 6666–6671.
34. Frey, G. L.; Tenne, R.; Matthews, M. J.; Dresselhaus, M.; Dresselhaus, G. Raman and Resonance Raman Investigation of MoS_2 Nanoparticles. *Phys. Rev. B* **1999**, *60*, 2883–2892.
35. Wilcoxon, J.; Newcomer, P.; Samara, G. Synthesis and Optical Properties of MoS and Isomorphous Nanoclusters in the Quantum Confinement Regime. *J. Appl. Phys.* **1997**, *81*, 7934–7944.
36. Luther, J. M.; Jain, P. K.; Ewers, T.; Alivisatos, A. P. Localized Surface Plasmon Resonances Arising from Free Carriers in Doped Quantum Dots. *Nat. Mater.* **2011**, *10*, 361–366.
37. Yoon, Y.; Ganapathi, K.; Salahuddin, S. How Good Can Monolayer MoS_2 Transistors Be? *Nano Lett.* **2011**, *11*, 3768–3773.
38. Another resonance at a lower frequency is expected due to the second (and third) shape parameter (equation 1.2); however, due to its interference with exciton C, it is very hard to distinguish between them.
39. Levi, R.; Bitton, O.; Leitus, G.; Tenne, R.; Joselevich, E. Field-Effect Transistors Based on Ws_2 Nanotubes with High Current-Carrying Capacity. *Nano Lett.* **2013**, *13*, 3736–3741.
40. Shahar, C.; Zbaida, D.; Rapoport, L.; Cohen, H.; Bendikov, T.; Tannous, J.; Dassenoy, F.; Tenne, R. Surface Functionalization of WS_2 Fullerene-like Nanoparticles. *Langmuir* **2009**, *26*, 4409–4414.
41. Shim, M.; Guyot-Sionnest, P. Organic-Capped ZnO Nanocrystals: Synthesis and n-Type Character. *J. Am. Chem. Soc.* **2001**, *123*, 11651–11654.
42. Schimpf, A. M.; Gunthardt, C. E.; Rinehart, J. D.; Mayer, J. M.; Gamelin, D. R. Controlling Carrier Densities In Photochemically Reduced Colloidal ZnO Nanocrystals: Size Dependence and Role of the Hole Quencher. *J. Am. Chem. Soc.* **2013**, *135*, 16569–16577.
43. Cohn, A. W.; Janßen, N.; Mayer, J. M.; Gamelin, D. R. Photocharging ZnO Nanocrystals: Picosecond Hole Capture, Electron Accumulation, and Auger Recombination. *J. Phys. Chem. C* **2012**, *116*, 20633–20642.
44. Faucheaux, J. A.; Jain, P. K. Plasmons in Photocharged ZnO Nanocrystals Revealing the Nature of Charge Dynamics. *J. Phys. Chem. Lett.* **2013**, *4*, 3024–3030.
45. Itzhakov, S.; Shen, H.; Buhbut, S.; Lin, H.; Oron, D. Type-II Quantum-Dot-Sensitized Solar Cell Spanning the Visible and Near-Infrared Spectrum. *J. Phys. Chem. C* **2013**, *117*, 22203–22210.
46. Sun, Q. C.; Xu, X.; Vergara, L.; Rosentsveig, R.; Musfeldt, J. Dynamical Charge and Structural Strain in Inorganic Fullerenelike MoS_2 Nanoparticles. *Phys. Rev. B* **2009**, *79*, 205405(6).
47. Coehoorn, R.; Haas, C.; De Groot, R. Electronic Structure of $MoSe_2$, MoS_2, and WSe_2. II. The Nature of the Optical Band Gaps. *Phys. Rev. B* **1987**, *35*, 6203–6206.
48. Böker, T.; Severin, R.; Müller, A.; Janowitz, C.; Manzke, R.; Voß, D.; Krüger, P.; Mazur, A.; Pollmann, J. Band Structure of MoS_2, $MoSe_2$, and A-$MoTe_2$: Angle-Resolved Photoelectron Spectroscopy and *Ab Initio* Calculations. *Phys. Rev. B* **2001**, *64*, 235305(11).
49. Seifert, G.; Terrones, H.; Terrones, M.; Jungnickel, G.; Frauenheim, T. Structure and Electronic Properties of MoS_2 Nanotubes. *Phys. Rev. Lett.* **2000**, *85*, 146–149.
50. Sun, Q. C.; Yadgarov, L.; Rosentsveig, R.; Seifert, G.; Tenne, R.; Musfeldt, J. L. Observation of a Burstein−Moss Shift in Rhenium-Doped MoS_2 Nanoparticles. *ACS Nano* **2013**, *7*, 3506–3511.
51. Mak, K. F.; He, K.; Lee, C.; Lee, G. H.; Hone, J.; Heinz, T. F.; Shan, J. Tightly Bound Trions In Monolayer MoS_2. *Nat. Mater.* **2013**, *12*, 207–211.
52. Lee, P. A. *Optical And Electrical Properties*; D. Reidel Publishing Company: Dordrecht, The Netherlands, 1976; Vol. 4.
53. Acrivos, J. V.; Liang, W.; Wilson, J.; Yoffe, A. Optical Studies of Metal-Semiconductor Transmutations Produced by Intercalation. *J. Phys. C: Solid State Phys.* **1971**, *4*, L18–L19.
54. Pankove, J. I. *Optical Processes in Semi-Conductors*; Dover Publications: Mineola, NY, 1971.
55. Kam, K.; Parkinson, B. Detailed Photocurrent Spectroscopy of the Semiconducting Group VIB Transition Metal Dichalcogenides. *J. Phys. Chem.* **1982**, *86*, 463–467.
56. Moore, W. J. *Basic Physical Chemistry*, 4th ed.; Prentice-Hall Inc.: London, 1962.
57. Chen, T.; Pourmand, M.; Feizpour, A.; Cushman, B.; Reinhard, B. R. M. Tailoring Plasmon Coupling in Self-Assembled One-Dimensional Au Nanoparticle Chains through Simultaneous Control of Size and Gap Separation. *J. Phys. Chem. Lett.* **2013**, *4*, 2147–2152.
58. Jain, P. K.; Eustis, S.; El-Sayed, M. A. Plasmon Coupling in Nanorod Assemblies: Optical Absorption, Discrete Dipole Approximation Simulation, and Exciton-Coupling Model. *J. Phys. Chem. B* **2006**, *110*, 18243–18253.
59. Fisher, M. L.; Colic, M.; Rao, M. P.; Lange, F. F. Effect of Silica Nanoparticle Size on the Stability of Alumina/Silica Suspensions. *J. Am. Ceram. Soc.* **2001**, *84*, 713–718.
60. Kosmulski, M. The pH-Dependent Surface Charging and the Points of Zero Charge. *J. Colloid Interface Sci.* **2002**, *253*, 77–87.
61. Suzuki, K. Quantaurus-QY: Absolute Photoluminescence Quantum Yield Spectrometer. *Nat. Photonics* **2011**, 5.
62. Ramakrishna Matte, H. S. S.; Gomathi, A.; Manna, A. K.; Late, D. J.; Datta, R.; Pati, S. K.; Rao, C. N. R. MoS_2 and WS_2 Analogues of Graphene. *Angew. Chem.* **2010**, *122*, 4153–4156.